Short Title: GFP-based cGMP sensor for imaging in an intact animal

Full Title: Robust and sensitive GFP-based cGMP sensor for real time imaging in intact *Caenorhabditis elegans*

Authors: Sarah Woldemariam[1,2], Jatin Nagpal[3,#a], Joy Li[4,#b], Martin W. Schneider[3], Raakhee Shankar[4,#c], Mary Futey[2,#d], Aruna Varshney[4], Kristine Andersen[4,#e], Benjamin Barsi-Rhyne[6,#b], Alan Tran[4,#f], Wagner Steuer Costa[3], Chantal Brueggemann[2,#g], O. Scott Hamilton[5], Denise M. Ferkey[6], Miri VanHoven[4], Alexander Gottschalk[3], Noelle L'Etoile[2,*]

Affiliations:

[1] Chemistry and Chemical Biology Graduate Program, University of California, San Francisco, San Francisco, CA 94158

[2] Department of Cell and Tissue Biology, University of California, San Francisco, San Francisco, CA 94143

[3] Department of Membrane Molecular Biology and Neurobiology, The Goethe University, Frankfurt, Germany

[4] Department of Biological Sciences, San Jose State University, San Jose, CA 95192

[5] Center for Neuroscience, University of California, Davis, Davis, CA 95618

[6] Department of Biology, State University of New York at Buffalo, Buffalo, NY 14260

[#a]Current Address: German Resilience Center, University Medical Center of the Johannes Gutenberg University Mainz, Mainz, Germany

[#b]Current Address: Tetrad Graduate Program, University of California, San Francisco, San Francisco, CA 94158

[#c]Current Address: Cellular and Molecular Biology Program, University of Wisconsin – Madison, Madison, WI 53706

[#d]Current Address: Faculty for International Students, Lobachevsky University, Nizhny Novgorod, Russia

[#e]Current Address: Peace Corps, Moshi Town, Tanzania

[#f]Current Address: School of Pharmacy, University of California, San Francisco, San Francisco, CA 94143

[#g]Current Address: European Molecular Biology Laboratory, Heidelberg, Germany

*Corresponding author

E-mail: noelle.letoile@ucsf.edu

Abstract

cGMP is a ubiquitous second messenger that plays a role in sensory signaling and plasticity through its regulation of ion channels and kinases. Previous studies that primarily used genetic and biochemical tools suggest that cGMP is spatiotemporally regulated in multiple sensory modalities, including light, heat, gases, salt and odor. FRET- and GFP-based cGMP sensors were developed to visualize cGMP in primary cell culture and *Caenorhabditis elegans* to corroborate these findings. While a FRET-based sensor has been used in an intact animal to visualize cGMP, the requirement of a multiple emission system limits its ability to be used on its own as well as with other sensors and

fluorescent markers. Here, we demonstrate that WincG2, a codon-optimized version of the cpEGFP-based cGMP sensor FlincG3, can be used in *C. elegans* to visualize rapidly changing cGMP levels in living, behaving animals using a single fluorophore. We coexpressed the sensor with the blue light-activated guanylyl cyclases BeCyclOp and bPGC in body wall muscles and found that the rate of WincG2 fluorescence correlated with the rate of cGMP production by each cyclase. Furthermore, we show that WincG2 responds linearly upon NaCl concentration changes and SDS presentation in the cell bodies of the gustatory neuron ASER and the nociceptive phasmid neuron PHB, respectively. Intriguingly, WincG2 fluorescence in the ASER cell body decreased in response to a NaCl concentration downstep and either stopped decreasing or increased in response to a NaCl concentration upstep, which is opposite in sign to previously published calcium recordings. These results illustrate that WincG2 can be used to report rapidly changing cGMP levels in an intact animal and that the reporter can potentially reveal unexpected spatiotemporal landscapes of cGMP in response to stimuli.

Author Summary

cGMP is a second messenger that plays an important role in sensory signaling and neural plasticity. Previous genetic and biochemical studies indirectly suggest that cGMP is spatiotemporally regulated in neurons to modulate neural activity. While a FRET-based sensor for cGMP has been used in intact *Caenorhabditis elegans* to examine its spatiotemporal regulation in neurobiological processes, its use has been limited due to the complicated setup required to image this type of sensor. Here, we describe a GFP-based cGMP sensor that has been codon optimized for use in *C. elegans* and

demonstrate that it responds robustly and reliably to endogenously changing cGMP levels. We show that the sensor responds to cGMP production by coexpressing it with blue light-activated guanylyl cyclases, and we show that it responds to NaCl and sodium dodecyl sulfate when expressed in a gustatory and nociceptive neuron, respectively. We think that this sensor can be used to investigate the spatiotemporal regulation of cGMP in neurons and its relationship to neural activity.

Introduction

The canonical second messenger molecule cGMP (cyclic guanosine monophosphate) regulates richly diverse functions in an animal's nervous system. cGMP signaling underlies the outgrowth of axons and the transduction of light, scent and other environmental cues to electrical signals in the brain [1]. Because so many neurobiological processes revolve around cGMP, having a robust, easy to use visual reporter for cGMP with precise temporal and spatial fidelity is critical to complement the primarily pharmacological, biochemical and genetic approaches used to study this second messenger's role in these processes. Such a reporter can be used to illuminate how producers and regulators of cGMP shape the landscape of this cyclic nucleotide in neurons.

Since cGMP is used in diverse cell types as a second messenger, its levels need to be regulated in ways that serve the cells' distinct functions. cGMP production can be regulated directly by stimuli such as ions, peptides, temperature and gases that interact with guanylyl cyclases (GCs) that convert GTP to cyclic GMP [2–8]. Recent evidence suggests that stimuli such as ions, peptides, Gα and temperature appear to largely

93 regulate transmembrane receptor guanylyl cyclases (rGCs), while membrane permeable
94 gases such as nitric oxide, carbon dioxide and oxygen have been shown to directly
95 activate soluble guanylyl cyclases (sGCs) [6–8]. Opposing the activity of GCs are
96 phosphodiesterases (PDEs) that hydrolyze cGMP; they can be regulated by cGMP,
97 cAMP, Ca^{2+}, kinases and the γ subunit of heteromeric G proteins [9–11]. cGMP effectors,
98 including cyclic nucleotide-gated channels and kinases, can act rapidly by changing the
99 membrane potential of a cell (e.g. the visual system); they can also have slower, more
100 long lasting effects on gene expression [12,13]. Thus, the precise subcellular localization
101 of GC and PDE proteins and their temporally regulated activities are likely to produce a
102 complex and dynamic landscape of varying cGMP levels and restricted localized
103 activation of effector proteins.

104 In neurobiology, the spatial localization of cGMP signal transduction pathways
105 suggest that spatiotemporal regulation of cGMP could play a role in sensory transduction
106 and plasticity, which is likely to be different in distinct neurons [14,15]. To this end, the
107 transparent nematode *C. elegans* is an ideal model system to visualize cGMP in
108 neurobiological processes. While the use of genetic manipulations in this animal yielded
109 valuable insights into the role of cGMP in sensory transduction, a visual tool that
110 complements this approach has the potential to reveal how this neuromodulator is
111 spatiotemporally regulated in real time. For instance, while mutants lacking distinct,
112 functional rGCs revealed that cGMP signaling was required for sensing specific gustatory
113 cues and NaCl concentration cultivation preference in *C. elegans*, it is unclear whether
114 this second messenger is spatiotemporally regulated [3,4,16]. Additionally, while genetic
115 evidence suggests that the cGMP-dependent protein kinase EGL-4 and GCs regulate *C.*

116 *elegans'* sensitivity to quinine through the flow of cGMP from sensory neurons to the
117 nociceptive neuron ASH through gap junctions [17,18], a visual tool could greatly enhance
118 our understanding of the process and its dynamics. In another nociceptive neuron, PHB,
119 genetic evidence suggests that the G protein coupled receptor *srb-6* is required to sense
120 noxious liquids including sodium dodecyl sulfate (SDS) and dodecanoic acid [19], and
121 calcium recordings suggest that avoidance of isoamyl alcohol is at least partially mediated
122 by the cGMP-gated cation channel TAX-2/TAX-4, both suggesting that cGMP flux is
123 required for sensing some nociceptive cues [20]. Thus, genetic tools demonstrate the
124 importance of cGMP signaling in distinct sensory modalities, and a tool to visualize cGMP
125 fluxes with precise temporal and spatial fidelity could deepen our understanding of these
126 important processes, offering a more complete picture of the cGMP landscape and
127 dynamics in cells. Such a tool will provide an essential complementary approach to the
128 primarily genetic approaches that have been used to examine cGMP dynamics in this
129 animal [21].

130 Though a Förster resonance energy transfer (FRET)-based tool has been used to
131 this end, a single channel fluorophore tool provides additional flexibility as it would allow
132 for more wavelengths to be used, making it more amenable for visualization with other
133 reporters (e.g. calcium sensors and fluorescent markers for organelles). In AWC, this
134 FRET-based sensor showed compartmentalized cGMP dynamics in response to
135 odorants [22]. Additionally, in PQR, simultaneous imaging of the cGMP sensor with a
136 calcium sensor in response to a 7% to 21% increase in O_2 revealed that a decrease in
137 cGMP correlated with an increase in Ca^{2+}, suggesting potential compartmentalization of
138 cGMP dynamics [8]. While these studies demonstrate that the FRET-based sensor can

be used to visualize the cGMP landscape in neurons, the complexity of a multiple emission system might raise a barrier to its use. Thus, having a robust, single fluorophore sensor for cGMP will complement the use of calcium sensors in this animal, providing a way to investigate how the spatiotemporal regulation of cGMP influences neural activity *in vivo*. Such a tool would be maximally efficient for probing the interplay between cGMP and calcium dynamics within sensory compartments in this transparent organism.

Here, we show that WincG2 (**W**orm **In**dicator of **cG**MP – **2**), the *C. elegans* codon-optimized version of the GFP-based circularly permuted cGMP sensor FlincG3, reports cGMP dynamics *in vivo* in *C. elegans* [23]. We characterize the biochemical and biophysical properties of WincG2 upon cGMP binding *in vivo* by ectopically expressing the blue light- activated guanylyl cyclases BeCyclOp and bPGC in muscle cells [24]. Using the WincG2 reporter, we show for the first time that sensory stimulation of either gustatory or nociceptive neurons triggers cGMP changes. We demonstrate that cGMP reliably decreases in response to NaCl concentration downsteps and increases in response to NaCl concentration upsteps in the salt-sensing neuron, ASER, which is opposite in sign to calcium transients that increase in response to NaCl concentration downsteps [3,25,26]. Additionally, we demonstrate that cGMP flux can be observed in the phasmid PHB neurons in response to a repulsive stimulus. Our results demonstrate that the GFP-based WincG2 is a versatile tool for the study of cGMP dynamics in different sensory modalities in intact animals using a single fluorophore.

Results

161 **WincG2 is a codon-optimized circularly permuted cGMP sensor derived from the**
162 **mammalian sensor, FlincG3**

163 WincG2, a genetically-encoded, circularly permuted EGFP-based cGMP sensor, is the
164 *C. elegans* codon-optimized version of FlincG3, which was initially characterized both *in*
165 *vitro* and in cell lines [23]. FlincG3 is based on FlincG, an earlier version of the sensor.
166 Like FlincG, FlincG3 contains the N-terminal region of protein kinase G (PKG) I α, which
167 is comprised of two cGMP-binding domains that bind cGMP cooperatively. The first 77
168 amino acids of the N-terminal region of the cGMP-binding domain were deleted to prevent
169 interactions with endogenous PKG [27]. This region of PKG I α is appended to the N-
170 terminus of circularly permuted EGFP (cpEGFP) [23,27]. In the presence of cGMP,
171 FlincG3 fluorescence increases, presumably due to the conformational changes of the
172 sensor upon cGMP binding that allow the beta barrel of GFP to form and create the
173 appropriate environment for fluorophore maturation [23,27]. The response amplitude of
174 the FlincG3 sensor to cGMP was enhanced by a M335K substitution located outside the
175 beta barrel of the cpEGFP domain (Fig 1) [23]. FlincG exhibits rapid kinetics, and FlincG3
176 retains this property as it rapidly detects changes in endogenous cGMP levels in the
177 nanomolar to low micromolar range in response to nitric oxide when expressed in
178 $HEK_{GC/PDE5}$ cells [23,27]. Additionally, FlincG3 fluorescence increases *in vitro* in response
179 to a 230-fold lower concentration of cGMP than cAMP, suggesting that it preferentially
180 binds to cGMP [23]. For our study we codon optimized FlincG3 for *C. elegans* and
181 inserted it into a standard *C. elegans* expression vector (Fig 1).
182

Stimulation of blue light-activated guanylyl cyclases increases WincG2 fluorescence

To test whether WincG2 can detect rapid changes in cGMP levels in an intact animal, we utilized the *C. elegans* body wall muscle cells, which lack most endogenous GCs. We coexpressed the reporter along with heterologous light-inducible GCs that have different cGMP production rates [24,28]. BeCyclOp is a microbial rhodopsin from *Blastocladiella emersonii* that is linked to a cytosolic GC domain (Fig 2A). It detects photons by absorption using the retinal chromophore and transmits this signal into activation of the GC domain [24]. bPGC (*Beggiatoa sp.* photoactivated guanylyl cyclase) is a BLUF-domain photosensor that is coupled to a GC domain (Fig 2C). It originates from bPAC (*Beggiatoa sp.* photoactivated adenylyl cyclase) that was mutated to generate cGMP rather than cAMP [28].

To test whether changes in WincG2 fluorescence and dynamics correspond with cGMP production by BeCyclOp, animals coexpressing WincG2 and BeCyclOp were grown with or without all-*trans* retinal (ATR), which is required for BeCyclOp activity. When WincG2 and BeCyclOp were coexpressed in body wall muscle cells in the presence of ATR, an acute increase in WincG2 fluorescence (peak $F\text{-}F_0/F_0$ = 0.218 ± 0.023 at 0.49s) was observed upon continuous blue light illumination, which activates BeCyclOp. This was followed by a slight decay over the duration of the recording (Fig 2B: top green trace). By contrast, animals grown without ATR and thus having no BeCyclOp activation exhibited an apparent decrease in WincG2 fluorescence ($F\text{-}F_0/F_0$ plateaued at approximately -0.310 to -0.312 beginning at 8.98s) when exposed to blue light (Fig 2B: bottom blue trace). The initial signal decayed; $F\text{-}F_0$ became negative, then plateaued and

remained steady for the duration of the recording. Notably, the initial fluorescence intensity F_0 (as measured in the absence of the rhodopsin cofactor ATR; bottom blue trace in Fig 2B) exhibited a rapid drop, possibly due to photoswitching behavior that was previously observed for other fluorescent proteins [29,30]. Taken together, we interpret these results to indicate that WincG2 fluorescence correlates with activation of BeCyclOp by blue light.

bPGC, a blue light-activated GC derived from the corresponding adenylyl cyclase bPAC (also known as BlaC), produces 50-fold less cGMP per unit time relative to BeCyclOp [24,28]. WincG2 fluorescence increased in the order of minutes upon continuous activation of bPGC with blue light (peak $F\text{-}F_0/F_0 = 0.122 \pm 0.023$ at 145.2 s) (Fig 2D). Note that at the onset of blue light illumination, WincG2 fluorescence increased, then decreased rapidly; this is presumably the same rapid photoswitching observed in the BeCyclOp experiment (the time constants for decay of the signal were essentially identical: 0.383 s for the experiment in Fig 2B, and 0.297 for the experiment in Fig 2D, in line with the hypothesis that this due to the same photophysical process). We chose F_0 after this photoswitching at 1 second after light onset (Fig 2D: inset). At this time, meaningful amounts of cGMP begin to develop, as judged from experiments in which bPGC was coexpressed in body wall muscle with the cGMP-gated cation channel TAX-2/TAX-4; muscle contractions from ion influx begin to be observable after 1 second of blue light (S1 Fig).

After photoswitching, we observed a slow rise in WincG2 fluorescence, which we interpret to be due to the slower kinetics of bPGC relative to BeCyclOp. By contrast, WincG2 fluorescence increased acutely upon activation of BeCyclOp, suggesting that the

rate of change of WincG2 fluorescence correlates with the rate of cGMP production by each GC.

Bhargava *et al.* showed that FlincG3 has a 230-fold lower EC_{50} for cGMP relative to cAMP [23]. To assess whether WincG2 fluorescence changes with increasing cAMP levels *in vivo*, WincG2 was coexpressed with bPAC, a bacterial blue light-activated adenylyl cyclase, in body wall muscle cells (Fig 2E) [31]. Following a fast drop in fluorescence, these animals showed a 10% increase in WincG2 fluorescence upon blue light stimulation of bPAC that peaked and decayed in a manner similar to that of the WincG2 response to BeCyclOp, albeit with slightly slower kinetics (Fig 2F). Thus, WincG2 appears to respond to cAMP. Indeed, bPAC is an efficient adenylyl cyclase that produces cAMP at the rate of 10 ± 2 nmol per minute per mg. Thus, it is not surprising that WincG2 responds to the high production of cAMP by bPAC [31]. Since there are no amino acid changes between WincG2 and FlincG3, it is expected that WincG2 is also activated more effectively by cGMP relative to cAMP. However, these results indicate that it is important to control for WincG2 response to cAMP.

WincG2 fluorescence in ASER cell body changes in response to NaCl concentration steps and depends on the rGC GCY-22

Genetic and calcium imaging studies indirectly suggest that cGMP in the gustatory neuron ASER mediates both acute sensation of NaCl removal and the food-mediated gradual resetting of NaCl cultivation preference [16,25]. ASER expresses multiple rGCs and may use cGMP to gate the cyclic nucleotide-gated TAX-2/TAX-4 cation channel upon NaCl concentration changes [3]. Consistent with this hypothesis, NaCl downsteps trigger an influx of calcium into ASER which was blocked in animals lacking TAX-2 or TAX-4

[25]. Additionally, a study indicating that cGMP could be a putative second messenger in ASER revealed that loss of the rGC GCY-22 blunts chemotaxis to Cl^- [4]. This suggests that cGMP levels could be modulated by changes in NaCl concentration [3].

To explore this hypothesis, we expressed WincG2 in the ASE neuron pair and monitored the sensor's response in the ASER cell body to ten 10-second steps between 50 and 0 mM NaCl. WincG2 fluorescence decreased linearly (R^2 = 0.9962) in response to a 50 to 0 mM NaCl downstep and stopped decreasing in response to the first 0 to 50 mM NaCl upstep (Fig 3A: blue trace, bottom). The slopes between the first downstep and upstep are different ($p<0.00001$; see Materials and Methods for statistical analysis), suggesting that WincG2 responds quickly to changing NaCl concentrations (Fig 3B: first pair, blue).

To test whether changes in WincG2 fluorescence were due to changing NaCl concentrations or to the potential fluctuation in pressure due to the change in flow of the stimulus presentation stream, we examined the sensor's responses to ten 10-second switches of 50 mM NaCl. WincG2 fluorescence did not change in these animals in response to switching (Fig 3A: pink trace, top; Fig 3B: second pair, pink). Additionally, the slopes of the first downstep between animals recorded in response to changing NaCl concentration and animals recorded in response to simply switching the buffer stream are different ($p<0.00001$), suggesting that WincG2 fluorescence changes were due to NaCl concentration steps and not to fluctuations in fluid pressure on the exposed nose of the animal (Fig 3B).

WincG2 has a cGMP-binding motif that could also potentially accommodate cAMP, albeit with lower affinity [23,27]. To assess whether WincG2 fluorescence was dependent

on cGMP or cAMP, we recorded ASER WincG2 fluorescence in animals lacking the rGC GCY-22. Though other rGCs are expressed in ASER [3,16], loss of GCY-22 produces the most severe behavioral defects in Cl^- and NaCl chemotaxis [3]. Consistent with these findings and in contrast to wild-type animals, WincG2 fluorescence did not change in *gcy-22(tm2364)* animals in response to NaCl downsteps or upsteps (Fig 3A: teal trace, ns; Fig 3B: third pair, teal). This finding indicates that changes in WincG2 fluorescence require GCY-22 and likely result from changes in cGMP rather than cAMP.

Wild-type WincG2 fluorescence also increased relative to switch control and *gcy-22* animals in response to the second, third and fourth 0 to 50 mM NaCl upstep (Fig 3C and S2 Fig) and was dependent on both an actual change in NaCl concentration (Fig 3C, compare blue trace with pink trace, $p<0.0001$) and the rGC GCY-22 (Fig 3C, compare blue trace with teal trace, $p<0.05$). Together, these results suggest that WincG2 can report rapidly changing increases and decreases in endogenous cGMP levels.

Animals expressing WincG2 in ASER prefer higher NaCl concentrations relative to animals that do not express the reporter

C. elegans requires ASER activity to adjust their preferred NaCl concentration to the concentration at which they were last fed; if ASER is killed, the animal's movement is less directed in response to a linear NaCl gradient [26]. Plasticity requires NaCl sensation, which in turn requires cGMP signaling; thus it is not surprising that *gcy-22(tm2364)* animals which we showed to not respond to NaCl concentration changes (Fig 3) do not exhibit a preference for the concentration of NaCl at which they were cultivated [16]. To assess whether WincG2 expression affected an animal's ability to exhibit a preference for its cultivation NaCl concentration, the behavior of WincG2-expressing wild-type animals

were compared to their nontransgenic siblings that did not express the WincG2 array and wild-type animals. Animals were cultivated for approximately six hours in the presence of OP50 *E. coli* bacteria on an NGM plate containing 25 mM, 50 mM, or 100 mM NaCl, then placed onto a chemotaxis assay plate containing a NaCl gradient from approximately 40 to 90 mM NaCl (Fig 4A, adapted from [16]). A chemotaxis index (CI) of 1 indicates the animals' preference for the higher NaCl concentration, and a CI of -1 indicates the animals' preference for the lower NaCl concentration. Wild-type and nontransgenic siblings behaved as previously described; animals that were cultivated at 25 mM, 50 mM, and 100 mM NaCl had a CI approaching -1, 0 and 0.75, respectively (Fig 4B: first and second set of three bars, respectively) [16]. The WincG2-expressing animals' NaCl concentration preference at each cultivation NaCl concentration was higher, though not significantly different from wild-type animals (Fig 4B: third set of three bars); however, their preference for a higher NaCl concentration was significantly different from their nontransgenic siblings when they were cultivated at 100mM NaCl ($p<0.05$). Additionally, the animals' preference for a higher NaCl concentration seemed different from their nontransgenic siblings when they were cultivated at 50mM, though this was not significant ($p=0.15$), presumably due to variability of the transgenic animals' chemotaxis to NaCl when cultivated at 50mM. Other lines injected at the same concentration exhibited NaCl seeking behavior that was significantly different from both wild-type animals and their nontransgenic siblings (S3 Fig). This may indicate that WincG2 expression lowers free cGMP levels and therefore interferes with an aspect of cGMP dynamics in ASER that is required for food to reset the animals' preference to their cultivation NaCl concentration.

320 WincG2 fluorescence was recorded for the line that exhibited behavior that was
321 not significantly different from wild-type animals. Importantly, in these animals, WincG2
322 fluorescence decreased linearly in response to a 50 to 0 mM NaCl downstep and stopped
323 decreasing in response to a 0 to 50 mM NaCl upstep, with the slopes between the first
324 downstep and upstep being different (Fig 4C: red trace, bottom; Fig 4D: second pair, red;
325 $p<0.00001$). This finding is similar to that observed with WincG2 injected at a lower
326 concentration (Fig 4D: first pair, blue; note that these data points are reproduced from Fig
327 3A: blue trace, bottom and Fig 3B: first pair, blue, respectively). The slopes of the first
328 downstep of wild-type animals injected at a lower versus higher concentration are not
329 different, indicating that the concentrations injected did not influence recordings (Fig 4D:
330 compare first blue trace with third red trace; p ns). Thus, though WincG2 reliably reports
331 the stimulus-induced changes in the gustatory sensory neuron ASER, its expression may
332 subtly alter behavior and this must be controlled for by comparing behavior in transgenic
333 lines to the non-transgenic siblings.
334
335 **WincG2 fluorescence increases in PHB chemosensory tail neurons in response to**
336 **SDS**
337 To examine the ability of WincG2 to report cGMP changes in a neuron with a
338 different modality, we expressed WincG2 in the nociceptive PHB neurons, which had
339 been predicted to use cGMP as a second messenger. The PHBs are a pair of bilaterally
340 symmetric sensory neurons located in the lumbar ganglia that extend ciliated dendrites
341 into the phasmid structures within the tail of *C. elegans*. PHB neurons are chemosensory
342 cells that are required for the avoidance of noxious chemicals such as SDS, dodecanoic

343 acid and other cues (Fig 5A) [19,20,32,33]. TAX-4 is required for PHB-mediated SDS
344 avoidance (Fig 5C), and calcium imaging has shown that PHB responds to SDS [20]. This
345 suggests that PHB may exhibit changes in cGMP levels in response to SDS that could
346 be monitored by recording changes in WincG2 fluorescence.

347 To test whether WincG2 affects the function of the PHB circuit, SDS response
348 assays (Fig 5B) were performed on wild-type animals and animals expressing WincG2 in
349 PHB neurons. On average, wild-type animals halt movement into a drop of 1 mM SDS in
350 less than a second. If PHB function is impaired, as in *tax-4* mutants, animals continue
351 moving into a drop of SDS as if it were a control buffer (M13). This increases the relative
352 response index to approximately 300% (Fig 5C). We found that behavioral responses to
353 SDS were unaffected by WincG2 expression, indicating that WincG2 does not affect PHB
354 function (Fig 5C).

355 To determine if cGMP changes in PHB neurons could be detected using WincG2,
356 the sensor's fluorescence in the cell body was measured in animals that were first
357 exposed to control buffer (M13), then to 1 mM SDS in M13 buffer. WincG2 fluorescence
358 remained largely steady in the absence of 1 mM SDS, but began to increase linearly
359 (R^2=0.9633) upon exposure to 1 mM SDS (Fig 5D). The area of the curve for the traces
360 before and after SDS presentation is different (permutation test, $p<0.00001$), which
361 suggests that cGMP increases in response to SDS and that WincG2 responds acutely to
362 endogenously produced cGMP that is induced by an external stimulus (Fig 5E).

363

364 **Discussion**

365 **WincG2 is a sensor for cGMP dynamics in *C. elegans***

366 The cGMP sensor WincG2 was successfully used to monitor the dynamics of this
367 second messenger in a number of cells in *C. elegans*. First, WincG2 was used to monitor
368 the kinetics of cGMP production in body wall muscles that lack most endogenous GCs.
369 The rate of increase in WincG2 fluorescence corresponded with the rate of cGMP
370 produced by coexpressed blue light-activated GCs. WincG2 fluorescence increased
371 within less than a second of activation of BeCyclOp, which produces 17 cGMP molecules
372 per second. In contrast, WincG2 fluorescence increased in the order of minutes upon
373 activation of bPGC, which produces cGMP at a 50-fold lower rate relative to BeCyclOp
374 [24]. WincG2 fluorescence slightly increased in the presence of cAMP in *C. elegans* in
375 response to activation of bPAC. Thus, care must be taken to control for fluctuations in
376 cAMP by imaging in backgrounds that lack cGMP production. The high rate of cAMP
377 production due to bPAC, however, is likely exceeding any intrinsic cAMP production by
378 several fold, thus side effects from intrinsic cAMP fluctuation may affect cGMP imaging
379 only to a minor extent.
380

381 **WincG2 reveals cGMP dynamics in sensory neurons that use cGMP as a second**
382 **messenger for sensory stimuli**

383 We expressed WincG2 in sensory neurons that use cGMP as a second messenger
384 and found that the sensor responds robustly to changing stimulus presentation. In the
385 gustatory neuron ASER, changes in WincG2 fluorescence in response to repeated NaCl
386 concentration steps suggest that the sensor can respond reliably to changing cGMP
387 levels, providing, for the first time, visual evidence that cGMP levels in ASER are
388 modulated by NaCl concentration changes. Importantly, we demonstrated that WincG2

fluorescence changes require the rGC GCY-22. This has two implications: 1) the sensor responds to cGMP in a physiologically relevant setting and 2) GCY-22 seems to be the primary rGC that produces cGMP for the NaCl response. Interestingly, the changes we observe in WincG2 fluorescence in ASER suggest that cGMP levels may be inversely correlated with calcium in response to a NaCl concentration change. Previously reported genetic and calcium imaging evidence suggested that cGMP levels would directly correlate with calcium levels; cGMP is hypothesized to bind and open the TAX-2/TAX-4 cyclic nucleotide-gated cation channel to allow for calcium influx [25]. A recent cryo-EM study showed that cGMP gates the homomeric TAX-4 channel in the open state [34]. Additionally, physiological investigations of the heterologously expressed heteromeric TAX-2/TAX-4 cation channel indicated that it opens in response to cGMP binding [35,36]. The unexpected result that WincG2 fluorescence decreases in response to NaCl downsteps could be due to the tight regulation of cGMP levels by phosphodiesterases. Resolution of this apparent paradox, however, awaits further investigation.

In the nociceptive phasmid neuron PHB, genetic evidence suggesting that it uses cGMP to signal the presence of SDS was corroborated by changes in WincG2 fluorescence. This is the first visual evidence for a cGMP-based signal in PHB, showing that it increases in response to an environmental cue. Importantly, expression of WincG2 did not perturb the function of the phasmid neurons, as SDS repulsion was as robust in the WincG2-expressing line as in wild-type animals. This is in contrast to WincG2 expression in ASER, which caused a slight preference for higher NaCl concentrations but minimally affected the plasticity of the NaCl concentration cultivation preference.

412 **Prospects for optimizing WincG2 and extending its use**

413 Like WincG2, the first generation of calcium sensors affected the behavior of
414 neurons in which they were expressed: the FRET-based YC2.12 acted as a calcium
415 sponge, a function that was exploited by Ferkey et al. to study nociceptive signaling [37],
416 and the GFP-based GCaMP2.2 blocked olfactory plasticity (personal communication,
417 Brueggemann and L'Etoile). Mutations that increased the quantal yield of GCaMP
418 allowed the reporters to be expressed at lower levels that did not interfere with cellular
419 function, yet were bright enough for imaging. Indeed, if WincG2 was enhanced to mimic
420 the properties of GCaMP6s, which contains (among other mutations) a K78H mutation in
421 the cpEGFP domain that improved sensitivity relative to GCaMP3, the fluorescence might
422 be bright enough to allow for lower expression of this reporter and thus reduce the
423 possibility of it interfering with cellular functions [38]. Until such optimizations are made,
424 it will be necessary to select for lines that express WincG2 at the lowest levels that allow
425 for imaging thereby minimizing the potential for behavioral effects. Addition of a
426 subcellular localization signal may also mitigate off-target effects.

427 We think WincG2 could be acting as a cGMP sponge due to its effects on NaCl-
428 seeking behavior when expressed in ASE (Fig 5B). These behavioral results suggest that
429 WincG2 could be altering free cGMP levels in ASER, which could lead to tuning the NaCl
430 concentration cultivation preference to be higher relative to nontransgenic siblings and
431 wild-type animals. If WincG2 can be shown to act as a cGMP sponge, this could also be
432 exploited to specifically and locally perturb cGMP levels. For example, if one could
433 localize a non-fluorescent form of WincG2 at the cilia, this may perturb function in a

different way from when it is localized to the cell body. This would reveal specific functions for cGMP signals at the sensory dendrites that are different from those in the cell body.

Additionally, the subcellular landscape of cGMP can also be probed using WincG2. For instance, adding a small tag that localizes WincG2 to specific regions of the cell along with a red protein for ratiometric imaging may reveal important aspects of the subcellular landscape of cGMP.

Though FRET-based cGMP sensors have been useful for uncovering cGMP dynamics in biological processes in an intact animal [8,22], the single fluorophore WincG2 provides the possibility of using additional fluorophores of different wavelengths to mark subcellular regions. This advantage of WincG2 will provide a simple and powerful tool with which to visualize changes in cGMP concentration across the subcellular landscape. Additionally, the ability to simultaneously visualize cGMP and calcium by using WincG2 with a red calcium sensor will allow us to investigate the dynamics of these second messengers at any marked subcellular location [39]. Our results demonstrate that WincG2 can be used to rapidly and specifically measure cGMP dynamics in the intact, behaving organism.

Materials and Methods

Molecular Biology

FlincG3 was codon optimized by Genscript for use in *C. elegans*. The *C. elegans* codon-optimized FlincG3, WincG2, was inserted into a worm specific expression (Fire) vector, pPD95.75, which facilitates transcription and translation of the sensor by providing worm specific introns [40].

The *gcy-5* promoter (2003 bp upstream of start site) was inserted using XbaI and EagI into pPD95.75 to make *gcy-5p*::WincG2. *myo-3p*::CyclOp::SL2::mCherry was made as described [24]. The plasmid *gcy-5p*::WincG2 was digested with XbaI and PciI and the *gcy-5* promoter fragment was replaced with the *myo-3* promoter fragment to yield the *myo-3p*::WincG2 plasmid construct.

pCFJ104 [*myo-3p*::mCherry::unc-54] was a gift from Erik Jorgensen (Addgene plasmid # 19328) [41]. To generate *myo-3p*::bPAC::SL2::mCherry, a 1193 bp long bPAC fragment was amplified using primers 5'-TCCATCTAGAGGATCCTTCCGCATCTCTTGTTCAAGGG-3' and 5'-CAGCGGTACCGTCGACTTACTTGTCGTTTTCCAGGGTCTG-3'. This was ligated into *myo-3p*::SL2::mCherry backbone, obtained by digestion with BamHI and SalI, using 'in-fusion cloning' (Clontech). To generate *myo-3p*::bPGC::SL2::mCherry, a 3486 bp long *myo-3p*::bPGC fragment was amplified using primers 5'-ATTACGCCAAGCTTGCGGCTATAATAAGTTCTTGAA-3' and 5'-TACCGTCGACGCTAGTTACTTGTCGTTTTCCAGGG-3'. This was ligated into a SL2::mCherry backbone, obtained by digestion with NheI and SphI, using 'in-fusion cloning' (Clontech).

To generate the *nlp-1p*::WincG2 construct, WincG2 from *gcy-5p::*WincG2 was inserted into the vector *nlp-1p*::pSMΔ [42] using the NEBuilder High-Fidelity DNA Assembly Cloning Kit (NEB) and the following primers: MVP598 WincG FWD (5'-ggattggccaaaggacATGGCACACCACCACCAC-3'), MPV599 WincG REV (5'-ggtcctcctgaaaatgttcTTATCGTCCGAATCCTCCG-3'), MVP597 *pSMΔ::nlp-1p* FWD (5'-

GAACATTTTCAGGAGGACCC-3'), and MVP596 *nlp-1p::pSM*Δ REV (5'-GTCCTTTGGCCAATCCCG-3'). The construct was then sequence-verified.

To generate the *flp-6p*::WincG2 construct, the *flp-6* promoter fragment was amplified from *flp-6p*::GCaMP6, a gift from the Lockery lab, using the primers 5'-ATTACGCCAAGCTTGCATGGCAGCGCTTGACTTCTGATG-3' and 5'-CCGGGGATCCTCTAGTGCAGGCATGCAAGCTTGTC-3'. The plasmid *nlp-1p*::WincG2 was digested with XbaI and SphI-HF and the *nlp-1* promoter fragment was replaced with the *flp-6* promoter fragment to yield the *flp-6p*::WincG2 plasmid construct using 'in-fusion' cloning (Clontech). The plasmid str-2::jRCaMP1b, a gift from the Bargmann lab, was digested with HindIII-HF and XmaI and str-2 was replaced with the *flp-6* promoter fragment to yield the *flp-6p*::jRCaMP1b plasmid construct using 'in-fusion' cloning (Clontech). The plasmid *str-2p*::jRGECO1a, a gift from the Bargmann lab, was digested with HindIII-HF and AscI and the *str-2* promoter fragment was replaced with the *flp-6* promoter fragment to yield the *flp-6p*::jRGECO1a plasmid construct using 'in-fusion' cloning (Clontech).

pJN55 [*myo-3p*::tax-2::GFP] and pJN58 [*myo-3p*::tax-4::GFP] plasmid construction have been previously reported [24]. pWSC13 [*myo-3p*::bPGC::eYFP]: pPD96.52 was cut with NheI and BamHI to yield a 6010 bp fragment, and bPGC synthetic construct, a gift from Peter Hegemann, was cut with BamHI and NheI to yield a 2106 bp fragment that was then inserted into cut pPD96.52. pJN59 [*myo-3p*::bPGC(K265D)::eYFP] : K265D was introduced into the parent plasmid pWSC13 (*myo-3p*::bPGC::eYFP) using the Q5 site-directed mutagenesis kit (New England Biolabs

Inc.) and primers oJN146 (5'-CCTGAAGATGGACCACGGCCTGC-3') and oJN147 (5'-CTGCTGCCCATGTTGCCC-3').

Transgenic Strains

Transgenic *C. elegans* were obtained by microinjection of DNA into the gonads of nematodes by standard procedures [43]. *ZX1921 (zxEx895[myo-3p::CyclOp::SL2::mCherry, myo-3p::WincG2])*: 15ng/µl *myo-3p*::CyclOp::SL2::mCherry and 15ng/µl *myo-3p*::WincG2 were microinjected into N2 background worms. *ZX1757 (zxEx893[myo-3p::mCherry, myo-3p::WincG2]):* 5 ng/µl *myo-3p*::mCherry and 20 ng/µl *myo-3p*::WincG2 were microinjected into N2 background worms. *ZX1922 (zxEx896[myo-3p::bPAC::SL2::mCherry, pmyo-3::WincG2]):* 15ng/µl *myo-3p*::bPAC::SL2::mCherry and 15ng/µl *myo-3p*::WincG2 were microinjected into N2 background worms. *ZX1756 (zxEx892[myo-3p::bPGC::SL2::mCherry, myo-3p::WincG2]):* 15ng/µl *myo-3p*::bPGC::SL2::mCherry and 15ng/µl *myo-3p*::WincG2 were microinjected into N2 background worms. *JZ1997 (ASE WincG2 in N2 injected with 15ng/µl WincG2)*: 15ng/µl *flp-6p*::WincG2, 30 ng/µl *flp-6p*::jRCaMP1b and 20ng/µl ofm-1::GFP were microinjected into N2 background worms. *JZ2089 (ASE WincG2 in N2 injected with 7.5 ng/µl WincG2)*: 7.5ng/µl *flp-6p*::WincG2, 60 ng/µl *flp-6p*::jRGECO1a and 20ng/µl ofm-1::GFP were microinjected into N2 background worms. *JZ2118 (ASE WincG2 in gcy-22)*: JZ2089 animals were crossed with OH4839 (*gcy-22(tm2364)*) animals to generate transgenic animals homozygous for *gcy-22(tm2364)*. *PHB WincG2 in N2*: MKV937 (*iyEx222*

524 [15ng/µL *nlp-1p::WincG2* and 45ng/µl *odr-1p::RFP* in N2 background worms]). *ZX1738*
525 *(zxEx886[myo-3p::bPGC::YFP, myo-3p::tax-2::GFP, myo-3p::tax-4::GFP])*: 15ng/µl *myo-*
526 *3p*::bPGC::YFP, 5 ng/µl *myo-3p*::tax-2::GFP and 5 ng/µl *myo-3p*::tax-4::GFP were injected
527 into *lite-1(ce314)* background worms.
528 *ZX1739 (zxEx887[myo-3p::bPGC(K265D)::YFP, myo-3p::tax-2::GFP, pmyo-3::tax-4::GFP])*:
529 15ng/µl *myo-3p*::bPGC(K265D)::YFP, 5 ng/µl *myo-3p*::tax-2::GFP and 5 ng/µl *myo-3p*::tax-
530 4::GFP were injected into *lite-1(ce314)* background worms.
531

532 **Imaging WincG2 coexpressed with BeCyclOp, bPGC or bPAC**

533 Transgenic strains were kept in the dark on standard NGM plates (5.5 cm
534 diameter; 8ml NGM) with OP50-1 bacteria with or without ATR at 20°C. Plates containing
535 ATR were prepared by spreading 200 µl of OP50-1 culture containing 100 mM of ATR
536 (diluted in ethanol). L4 animals were put on ATR plates overnight and young adults were
537 used for imaging the following day.

538 For cGMP/cAMP imaging, animals were immobilized on 10% M9 agar pads with
539 polystyrene beads (Polysciences, USA). The fluorescence measurements were
540 performed with a 25x oil objective (Zeiss 25x LCI-Plan / 0.8 Imm Corr DIC) on the inverted
541 microscope Axio Observer Z.1 equipped with two high-power light emitting diodes (LEDs;
542 470 and 590 nm wavelength, KSL 70, Rapp Optoelektronik, Germany) coupled via a
543 beam splitter and a double band pass excitation filter permitting wavelengths of
544 479/21 nm and 585/19 (F74-423 479/585 HC Dualband Filter AHF Analysentechnik) to
545 obtain simultaneous dual-wavelength illumination. DIC microscopy using white light
546 filtered with a red optical filter was used to focus on the body wall muscle cells prior to

video acquisition. The 470nm and 590 nm excitation was switched on simultaneously after the start of video acquisition. For bPGC experiments, yellow light was used to focus the cells, and thereafter the blue illumination was turned on. Fluorescence was acquired by an ORCA-Flash 4.0 sCMOS camera (Hamamatsu) through a Dual-View beam splitter (DV2, Photometrics) with a 540/25 nm emission filter used for WincG2 green channel and a 647/57 emission filter for mCherry red channel. Videos were acquired using µManager [44], and frames were taken at 100Hz (corresponding to exposure times of 10 ms) and 20Hz (for bPGC) with 4×4 spatial binning. The optical power was 3.3 mW/mm^2 at 470 nm and 2.6 mW/mm^2 at 590 nm.

Image analysis was performed in ImageJ (NIH). Regions of interest (ROIs) were drawn around single body wall muscle cells that did not show major movement and a region outside the animals was chosen as background ROI. The mean fluorescence intensity of the ROIs for both channels was analyzed with ImageJ. Background subtracted values were used to calculate the change in fluorescence intensity for each time point: $(F-F_0)/F_0$ where F represents the intensity at this time point and F_0 represents the peak intensity at the onset of light stimulation. For bPGC experiments, F_0 represents the intensity 5s after the onset of light stimulation.

Imaging WincG2 in ASER and PHB

WincG2 imaging was performed essentially as described for calcium imaging [17]. Briefly, for imaging ASER, day 1 adults grown at 20°C were transferred from NGM plates containing OP50 to a 35 mm x 10 mm petri dish containing chemotaxis buffer with 50 mM NaCl (25 mM K_3PO_4, pH 6.0, 1 mM $CaCl_2$, 1 mM $MgSO_4$, 50 mM NaCl, adjusted to 355

570 ± 2 mOsm with sorbitol). The worms were then placed in a microfluidic device that can
571 expose the animal to stimulus [45]. A Zeiss 40x air objective on an inverted microscope
572 (Zeiss Axiovert 200) was used for imaging, and images were taken at rate of 1Hz with a
573 blue light exposure time of 30 ms using an ORCA-Flash 2.8 camera (Hamamatsu) for a
574 total of 103 frames. Recordings were taken within eight minutes of the animal's exposure
575 to chemotaxis buffer with 50 mM NaCl, and the animals were subjected to either ten
576 second steps between chemotaxis buffer with 50 and 0 mM NaCl (each containing 1 mM
577 levamisole) or switches between chemotaxis buffer with 50 mM NaCl (each containing 1
578 mM levamisole (Sigma-Aldrich), and one containing fluorescein). Images were obtained
579 using µManager (Version 1.4.22). Fluorescence intensity was measured using ImageJ.
580 To calculate the fluorescence intensity at a given time point (F), the fluorescence intensity
581 from the region of interest (ROI) encompassing the neuron was subtracted from the
582 background ROI. The fluorescence intensity F of the first three frames was averaged to
583 calculate F_0. We used $\Delta F/F_0$ ($F-F_0/F_0$) to calculate the change in fluorescence intensity
584 at a given time point.

585 To image WincG2 in PHB neurons, animals were picked from NGM plates
586 containing OP50 onto a petri dish containing M13 control buffer, then placed tail-first into
587 the microfluidic device. They were exposed to control buffer for 15 seconds, and then to
588 1 mM SDS in M13 for 15 seconds. They were imaged at a rate of 2 Hz. To calculate the
589 fluorescence intensity of PHB at each frame, Image J was used to measure the total intensity
590 of the cell body. Background fluorescence was calculated by using ImageJ to measure the
591 minimum pixel value in the area surrounding the cell body, and this pixel value was multiplied
592 by the area of the cell body to get the total background. The total background was subtracted

593 from the total intensity of the cell body to calculate the fluorescence intensity. The PHB
594 WincG2 fluorescence intensities were adjusted for photobleaching using the following
595 method. The decrease in fluorescence during the first 29 frames when the animal was
596 exposed to control buffer was presumed to be due to photobleaching. Therefore, the average
597 difference between the values for the nth frame and the n+1th frame (up to the 29th frame)
598 were calculated, and this average photobleaching value was then added back to each value
599 in the series. F_0 was the average of the response to buffer adjusted for photobleaching
600 over the first 15 seconds, rather than only the first 3 data points.
601
602 **NaCl cultivation assay**
603 The NaCl cultivation assay was essentially performed as described [16]. Briefly,
604 day 1 animals grown at 20°C were transferred from OP50-containing NGM plates
605 containing 50 mM NaCl to OP50-containing NGM plates containing 25 mM, 50 mM, or
606 100 mM NaCl for approximately six hours before being placed on a chemotaxis assay
607 plate containing regions of higher and lower NaCl for 45 minutes. Afterward, worms were
608 stored in 4°C for at least 16 hours before calculating the chemotaxis index. Chemotaxis
609 index = [# animals at higher NaCl region – # animals at lower NaCl region]/ [# animals at
610 higher NaCl region + # animals at lower NaCl region + # animals outside origin].
611
612 **Behavioral assay response to the repellent SDS**
613 SDS dry drop behavioral assays were conducted by using a hair pick to touch each
614 worm on the nose to stimulate backward movement into a dry drop of 1 mM SDS in M13
615 buffer [32,33]. A dry drop is obtained by incubating an NGM plate overnight at 37°C so

that the SDS drop dries quickly into the plate, preventing wicking along the animal that might activate neurons in the head. An animal's response time was defined as the amount of time it backed into the dry drop before terminating backward movement. The average response time to the dry drop of dilute SDS in M13 buffer was compared to the average response time to a drop of control M13 buffer. A response index was calculated by dividing the average response time to SDS by the average response time to M13 buffer. *nlp-1p*::WincG2 and *tax-4* mutants were each compared to wild-type animals assayed on the same day, and the wild-type response index is normalized to 100%. At least 80 animals of each genotype were tested: 40 for a response to M13, and 40 for a response to SDS.

Muscle Contraction Assay

The muscle contraction assay was essentially performed as described [24]. L4 animals were exposed to 0.9 mW/mm^2 blue light (450-490 nm) for approximately 20 seconds, and relative body length was measured with a custom LabView script.

Statistical Analysis for ASER and PHB WincG2

To compare the sum of slope values of the first 50 to 0 mM NaCl downstep with the first 0 to 50 mM NaCl upstep, as well as the sum of slope values of the first 50 to 0 mM NaCl downstep and the second, third, and fourth 0 to 50 mM NaCl upstep, an approximate p-value ranked permutation test was performed on the data. To compare the sum of slope values of the first 50 to 0 mM NaCl downstep with the first 0 to 50 mM NaCl upstep, the sum of slopes for randomly rearranged data is calculated and ranked relative

to the sum of slopes for the first 50 to 0 mM NaCl downstep. For example, to compare the sum of slope values of the first 50 to 0 mM NaCl downstep with the first 0 to 50 mM NaCl upstep for wild-type animals, the 34 slope values of the first downstep and upstep were combined in a list then randomly rearranged, and the sum of the first 17 slope values of that randomly rearranged list was calculated and ranked relative to the sum of 17 slope values for the first 50 to 0 mM NaCl downstep. To compare the sum of slope values of the first 50 to 0 mM NaCl downstep between conditions, the sum of slopes for the randomly rearranged data is calculated and ranked relative to the sum of slopes for wild-type. For example, for comparing the sum of slope values of the first 50 to 0 mM NaCl downstep between wild-type and *gcy-22* animals, the 40 (n=17 for wild-type and n=23 for *gcy-22*) slope values were combined in a list then randomly rearranged, and the sum of the first 17 slope values of that randomly rearranged list was calculated and ranked relative to the sum of 17 slope values for wild-type. This type of statistical test was also performed for comparing the second, third, and fourth 0 to 50 mM NaCl upstep between conditions. The sum of slopes from at least 500,000 randomly selected permutations were calculated and ranked using a custom Python script. For comparing the sum of slope values of the first 50 to 0 mM NaCl downstep with the first 0 to 50 mM NaCl upstep for wild-type switch control; for comparing the sum of slope values for the first 50 to 0 mM NaCl downstep between wild-type and wild-type switch control; and for comparing the area under the curve for the first 30 frames of PHB WincG2 (corresponding to M13 buffer) with the next 30 frames of PHB WincG2 (corresponding to 1 mM SDS), an exact p-value ranked permutation test was performed. For this test, the sum of slopes for all possible permutations of the data was calculated and ranked using a custom Python script.

Author contributions

KA, WSC, MF, SW and MWS prepared reagents. JL, JN, BB-R, MWS, RS, AT and AV performed experiments. SW guided the project and performed experiments. OSH initiated the line of experimentation. AG, NDL and MV conceived the experiments and guided the project. DMF and CB helped guide the project. AG, NDL, JN, MV and SRW wrote the manuscript.

Acknowledgements: The authors would like to thank Martina Bremer and Saul Kato for statistical consults, as well as Cornelia Bargmann, Peter Hegemann, Erik Jorgensen and Shawn Lockery for reagents. The authors would also like to thank Sarah Nordquist and Piali Sengupta for guidance on writing the manuscript. NDL and MKV were supported by NIDCD R01 DC005991 and NINDS R01 NS087544-01; NDL and DMF by NIDCD R01 DC015758; AG by DFG (Deutsche Forschungsgemeinschaft) grants GO1011/4-2, GO1011/13-1 and EXC115; SW by Diversity Supplement NS87544 and 5T32DE007306-21.

References

1. Potter LR. Guanylyl cyclase structure, function and regulation. Cell Signal. 2011;23: 1921–1926. doi:10.1016/j.cellsig.2011.09.001

683 2. Yu S, Avery L, Baude E, Garbers DL. Guanylyl cyclase expression in specific
684 sensory neurons: a new family of chemosensory receptors. Proc Natl Acad Sci U S
685 A. 1997;94: 3384–3387.

686 3. Ortiz CO, Faumont S, Takayama J, Ahmed HK, Goldsmith AD, Pocock R, et al.
687 Lateralized gustatory behavior of *C. elegans* is controlled by specific receptor-type
688 guanylyl cyclases. Curr Biol CB. 2009;19: 996–1004. doi:10.1016/j.cub.2009.05.043

689 4. Smith HK, Luo L, O'Halloran D, Guo D, Huang X-Y, Samuel ADT, et al. Defining
690 specificity determinants of cGMP mediated gustatory sensory transduction in
691 *Caenorhabditis elegans*. Genetics. 2013;194: 885–901.
692 doi:10.1534/genetics.113.152660

693 5. Singhvi A, Liu B, Friedman CJ, Fong J, Lu Y, Huang X-Y, et al. A Glial K/Cl
694 Transporter Controls Neuronal Receptive Ending Shape by Chloride Inhibition of an
695 rGC. Cell. 2016;165: 936–948. doi:10.1016/j.cell.2016.03.026

696 6. Hallem EA, Spencer WC, McWhirter RD, Zeller G, Henz SR, Rätsch G, et al.
697 Receptor-type guanylate cyclase is required for carbon dioxide sensation by
698 *Caenorhabditis elegans*. Proc Natl Acad Sci U S A. 2011;108: 254–259.
699 doi:10.1073/pnas.1017354108

700 7. Lucas KA, Pitari GM, Kazerounian S, Ruiz-Stewart I, Park J, Schulz S, et al. Guanylyl
701 cyclases and signaling by cyclic GMP. Pharmacol Rev. 2000;52: 375–414.

8. Couto A, Oda S, Nikolaev VO, Soltesz Z, de Bono M. In vivo genetic dissection of O2-evoked cGMP dynamics in a *Caenorhabditis elegans* gas sensor. Proc Natl Acad Sci U S A. 2013;110: E3301-3310. doi:10.1073/pnas.1217428110

9. Conti M, Beavo J. Biochemistry and physiology of cyclic nucleotide phosphodiesterases: essential components in cyclic nucleotide signaling. Annu Rev Biochem. 2007;76: 481–511. doi:10.1146/annurev.biochem.76.060305.150444

10. Francis SH, Blount MA, Corbin JD. Mammalian cyclic nucleotide phosphodiesterases: molecular mechanisms and physiological functions. Physiol Rev. 2011;91: 651–690. doi:10.1152/physrev.00030.2010

11. Ahmad F, Murata T, Shimizu K, Degerman E, Maurice D, Manganiello V. Cyclic nucleotide phosphodiesterases: important signaling modulators and therapeutic targets. Oral Dis. 2015;21: e25-50. doi:10.1111/odi.12275

12. Lee JI, O'Halloran DM, Eastham-Anderson J, Juang B-T, Kaye JA, Scott Hamilton O, et al. Nuclear entry of a cGMP-dependent kinase converts transient into long-lasting olfactory adaptation. Proc Natl Acad Sci U S A. 2010;107: 6016–6021. doi:10.1073/pnas.1000866107

13. Juang B-T, Gu C, Starnes L, Palladino F, Goga A, Kennedy S, et al. Endogenous nuclear RNAi mediates behavioral adaptation to odor. Cell. 2013;154: 1010–1022. doi:10.1016/j.cell.2013.08.006

14. Gross OP, Pugh EN, Burns ME. cGMP in mouse rods: the spatiotemporal dynamics underlying single photon responses. Front Mol Neurosci. 2015;8: 6. doi:10.3389/fnmol.2015.00006

15. Mukhopadhyay S, Lu Y, Shaham S, Sengupta P. Sensory signaling-dependent remodeling of olfactory cilia architecture in *C. elegans*. Dev Cell. 2008;14: 762–774. doi:10.1016/j.devcel.2008.03.002

16. Kunitomo H, Sato H, Iwata R, Satoh Y, Ohno H, Yamada K, et al. Concentration memory-dependent synaptic plasticity of a taste circuit regulates salt concentration chemotaxis in *Caenorhabditis elegans*. Nat Commun. 2013;4: 2210. doi:10.1038/ncomms3210

17. Krzyzanowski MC, Brueggemann C, Ezak MJ, Wood JF, Michaels KL, Jackson CA, et al. The *C. elegans* cGMP-dependent protein kinase EGL-4 regulates nociceptive behavioral sensitivity. PLoS Genet. 2013;9: e1003619. doi:10.1371/journal.pgen.1003619

18. Krzyzanowski MC, Woldemariam S, Wood JF, Chaubey AH, Brueggemann C, Bowitch A, et al. Aversive Behavior in the Nematode *C. elegans* Is Modulated by cGMP and a Neuronal Gap Junction Network. PLoS Genet. 2016;12: e1006153. doi:10.1371/journal.pgen.1006153

19. Tran A, Tang A, O'Loughlin CT, Balistreri A, Chang E, Coto Villa D, et al. *C. elegans* avoids toxin-producing Streptomyces using a seven transmembrane domain chemosensory receptor. eLife. 2017;6. doi:10.7554/eLife.23770

20. Zou W, Cheng H, Li S, Yue X, Xue Y, Chen S, et al. Polymodal Responses in *C. elegans* Phasmid Neurons Rely on Multiple Intracellular and Intercellular Signaling Pathways. Sci Rep. 2017;7: 42295. doi:10.1038/srep42295

21. O'Halloran DM, Hamilton OS, Lee JI, Gallegos M, L'Etoile ND. Changes in cGMP levels affect the localization of EGL-4 in AWC in *Caenorhabditis elegans*. PloS One. 2012;7: e31614. doi:10.1371/journal.pone.0031614

22. Shidara H, Hotta K, Oka K. Compartmentalized cGMP Responses of Olfactory Sensory Neurons in *Caenorhabditis elegans*. J Neurosci Off J Soc Neurosci. 2017;37: 3753–3763. doi:10.1523/JNEUROSCI.2628-16.2017

23. Bhargava Y, Hampden-Smith K, Chachlaki K, Wood KC, Vernon J, Allerston CK, et al. Improved genetically-encoded, FlincG-type fluorescent biosensors for neural cGMP imaging. Front Mol Neurosci. 2013;6: 26. doi:10.3389/fnmol.2013.00026

24. Gao S, Nagpal J, Schneider MW, Kozjak-Pavlovic V, Nagel G, Gottschalk A. Optogenetic manipulation of cGMP in cells and animals by the tightly light-regulated guanylyl-cyclase opsin CyclOp. Nat Commun. 2015;6: 8046. doi:10.1038/ncomms9046

25. Suzuki H, Thiele TR, Faumont S, Ezcurra M, Lockery SR, Schafer WR. Functional asymmetry in *Caenorhabditis elegans* taste neurons and its computational role in chemotaxis. Nature. 2008;454: 114–117. doi:10.1038/nature06927

761 26. Luo L, Wen Q, Ren J, Hendricks M, Gershow M, Qin Y, et al. Dynamic encoding of
762 perception, memory, and movement in a *C. elegans* chemotaxis circuit. Neuron.
763 2014;82: 1115–1128. doi:10.1016/j.neuron.2014.05.010

764 27. Nausch LWM, Ledoux J, Bonev AD, Nelson MT, Dostmann WR. Differential
765 patterning of cGMP in vascular smooth muscle cells revealed by single GFP-linked
766 biosensors. Proc Natl Acad Sci U S A. 2008;105: 365–370.
767 doi:10.1073/pnas.0710387105

768 28. Ryu M-H, Moskvin OV, Siltberg-Liberles J, Gomelsky M. Natural and engineered
769 photoactivated nucleotidyl cyclases for optogenetic applications. J Biol Chem.
770 2010;285: 41501–41508. doi:10.1074/jbc.M110.177600

771 29. Shaner NC, Lin MZ, McKeown MR, Steinbach PA, Hazelwood KL, Davidson MW, et
772 al. Improving the photostability of bright monomeric orange and red fluorescent
773 proteins. Nat Methods. 2008;5: 545–551. doi:10.1038/nmeth.1209

774 30. Akerboom J, Carreras Calderón N, Tian L, Wabnig S, Prigge M, Tolö J, et al.
775 Genetically encoded calcium indicators for multi-color neural activity imaging and
776 combination with optogenetics. Front Mol Neurosci. 2013;6: 2.
777 doi:10.3389/fnmol.2013.00002

778 31. Stierl M, Stumpf P, Udwari D, Gueta R, Hagedorn R, Losi A, et al. Light modulation
779 of cellular cAMP by a small bacterial photoactivated adenylyl cyclase, bPAC, of the
780 soil bacterium *Beggiatoa*. J Biol Chem. 2011;286: 1181–1188.
781 doi:10.1074/jbc.M110.185496

782 32. Hilliard MA, Bargmann CI, Bazzicalupo P. *C. elegans* responds to chemical
783 repellents by integrating sensory inputs from the head and the tail. Curr Biol CB.
784 2002;12: 730–734.

785 33. Park J, Knezevich PL, Wung W, O'Hanlon SN, Goyal A, Benedetti KL, et al. A
786 conserved juxtacrine signal regulates synaptic partner recognition in *Caenorhabditis*
787 *elegans*. Neural Develop. 2011;6: 28. doi:10.1186/1749-8104-6-28

788 34. Li M, Zhou X, Wang S, Michailidis I, Gong Y, Su D, et al. Structure of a eukaryotic
789 cyclic-nucleotide-gated channel. Nature. 2017;542: 60–65.
790 doi:10.1038/nature20819

791 35. Komatsu H, Jin YH, L'Etoile N, Mori I, Bargmann CI, Akaike N, et al. Functional
792 reconstitution of a heteromeric cyclic nucleotide-gated channel of *Caenorhabditis*
793 *elegans* in cultured cells. Brain Res. 1999;821: 160–168.

794 36. O'Halloran DM, Altshuler-Keylin S, Zhang X-D, He C, Morales-Phan C, Yu Y, et al.
795 Contribution of the cyclic nucleotide gated channel subunit, CNG-3, to olfactory
796 plasticity in *Caenorhabditis elegans*. Sci Rep. 2017;7: 169. doi:10.1038/s41598-017-
797 00126-7

798 37. Ferkey DM, Hyde R, Haspel G, Dionne HM, Hess HA, Suzuki H, et al. *C. elegans* G
799 protein regulator RGS-3 controls sensitivity to sensory stimuli. Neuron. 2007;53: 39–
800 52. doi:10.1016/j.neuron.2006.11.015

801 38. Chen T-W, Wardill TJ, Sun Y, Pulver SR, Renninger SL, Baohan A, et al.
802 Ultrasensitive fluorescent proteins for imaging neuronal activity. Nature. 2013;499:
803 295–300. doi:10.1038/nature12354

804 39. Dana H, Mohar B, Sun Y, Narayan S, Gordus A, Hasseman JP, et al. Sensitive red
805 protein calcium indicators for imaging neural activity. eLife. 2016;5.
806 doi:10.7554/eLife.12727

807 40. Evans T, editor. Transformation and microinjection. WormBook: The Online Review
808 of C elegans Biology [Internet]. 2006.

809 41. Frøkjær-Jensen C, Wayne Davis M, Hopkins CE, Newman BJ, Thummel JM, Olesen
810 S-P, et al. Single-copy insertion of transgenes in *Caenorhabditis elegans*. Nat Genet.
811 2008;40: 1375–1383. doi:10.1038/ng.248

812 42. Barsi-Rhyne BJ, Miller KM, Vargas CT, Thomas AB, Park J, Bremer M, et al. Kinesin-
813 1 acts with netrin and DCC to maintain sensory neuron position in *Caenorhabditis*
814 *elegans*. Genetics. 2013;194: 175–187. doi:10.1534/genetics.113.149310

815 43. Fire A. Integrative transformation of *Caenorhabditis elegans*. EMBO J. 1986;5:
816 2673–2680.

817 44. Edelstein A, Amodaj N, Hoover K, Vale R, Stuurman N. Computer control of
818 microscopes using μManager. Curr Protoc Mol Biol Ed Frederick M Ausubel Al.
819 2010;Chapter 14: Unit14.20. doi:10.1002/0471142727.mb1420s92

45. Chronis N, Zimmer M, Bargmann CI. Microfluidics for in vivo imaging of neuronal and behavioral activity in *Caenorhabditis elegans*. Nat Methods. 2007;4: 727–731. doi:10.1038/nmeth1075

Figure Captions

Fig 1. WincG2 is a GFP-based cGMP sensor codon optimized for use in *C. elegans*.

WincG2 is the *C. elegans* codon-optimized version of the mammalian cGMP sensor FlincG3 (figured adapted from Garthwaite) [23]. This GFP-based sensor contains two in-tandem protein kinase G (PKG) I α cGMP binding domains that bind cGMP cooperatively (PKG1α (77-356); maroon); this regulatory PKG domain is attached to the N terminus of circularly permuted EGFP (cpEGFP; green). Changing the methionine at position 335, located outside the beta barrel of the cpEGFP domain, to lysine (M335K), improved the response amplitude of the sensor to cGMP [23]. GGTGGS is a linker between the two GFP halves. This linker, along with the 6xHis-tag region (H6) and the Tag Region, were retained from FlincG3. This *C. elegans* codon-optomized sensor, prepared by Genscript, was inserted into a worm-specific Fire vector, pPD95.75, which contains synthetic introns (SynIVS.A and SynIVS.L; blue) to facilitate expression, a multiple cloning site (MCS) and the 3' untranslated region of *unc-54* (*unc-54* 3' UTR; orange).

Fig 2. WincG2 fluorescence increases upon stimulation of blue light-activated guanylyl cyclases when coexpressed in body wall muscle cells.

(A) BeCyclOp is a fungal blue light-activated guanylyl cyclase that generates cGMP with a turnover rate of approximately 17 cGMP s^{-1} at 20°C [24].

(B) $(F-F_0)/F_0$ for WincG2 fluorescence intensity in *myo-3p*::CyclOp::SL2::mCherry*; myo-3p*::WincG2 animals grown in the absence and presence of all-*trans* retinal (ATR). n=6 for WincG2 fluorescence intensity without ATR (light green, bottom); n=5 for WincG2 fluorescence intensity with ATR (dark green, top). Inset shows raw traces and indicates F_0. (C) bPGC is a bacterial blue light-activated guanylyl cyclase containing a BLUF (blue light receptor using FAD) domain with an estimated turnover rate of 0.2 cGMP s^{-1} [28]. (D) $(F-F_0)/F_0$ for WincG2 fluorescence intensity in *myo-3p*::bPGC::SL2::mCherry; *myo-3p*::WincG2 animals (n=5, 27 ROIs). Inset shows raw traces and indicates F_0. (E) bPAC is a bacterial blue-light activated adenylyl cyclase containing a BLUF (blue light receptor using FAD) domain. *In vitro* cAMP production in the presence of blue light is 10 ± 2 nmol cAMP per minute per mg [31]. (F) $(F-F_0)/F_0$ for WincG2 fluorescence intensity in *myo-3p*::bPAC::SL2::mCherry, *myo-3p*::WincG2 animals. n=7. Inset shows average of traces during the first two seconds of recording.

Fig 3. WincG2 fluorescence in the ASER cell body changes linearly in response to 50 mM NaCl step changes and depends on the receptor guanylyl cyclase GCY-22.

(A) Average fluorescence response ($\Delta F/F_0$) of WincG2 in ASER cell body shown as traces responding to either 10 second steps between 50 and 0 mM NaCl or switch control (represented at the bottom of the panel). WincG2 fluorescence in wild-type (N2) animals

863 decreases linearly in response to a 50 to 0 mM NaCl downstep and stops decreasing in
864 response to a 0 to 50 mM NaCl upstep (blue trace, bottom). These responses are not
865 seen in *gcy-22(tm2364)* animals (teal trace, middle) or when wild-type animals are
866 exposed to switch control (pink trace, top). n=17, n=23 and n=11 for wild-type, *gcy-*
867 *22(tm2364)* and wild-type switch control, respectively. Regression analysis was applied
868 to the data for the first 50 to 0 mM NaCl downstep. R^2 = 0.9962, R^2 = 0.0436 and R^2 =
869 0.1515 for wild-type, *gcy-22 (tm2364)* and wild-type switch control, respectively. (B)
870 WincG2 fluorescence in the ASER cell body decreases in response to a 50 to 0 mM NaCl
871 downstep and stops decreasing in response to a 0 to 50 mM NaCl upstep in wild-type
872 animals. The slopes for the first 50 to 0 mM NaCl downstep between wild-type and *gcy-*
873 *22(tm2364)* animals are different (n = 17 (first set, blue; wild-type), n=23 (fifth set, teal;
874 *gcy-22*); permutation test p<0.00001). In wild-type animals, the slopes in response to the
875 first 50 to 0 mM NaCl down step are also different from those of the switch control (n= 17
876 (first set, blue; 50 mM NaCl downstep), n=11 (third set, pink; switch control); permutation
877 test p<0.00001). The slope values between the first 50 to 0 mM NaCl downstep and 0 to
878 50 mM NaCl upstep are different in wild-type animals (n=17; first pair, blue; permutation
879 test p<0.00001), as compared to those of the switch control in wild-type animals and *gcy-*
880 *22* animals, which were not different (n=11; second pair, pink and n=23; third pair, teal,
881 respectively). See Materials and Methods for details of statistical analysis. (C) WincG2
882 fluorescence in the ASER cell body increases in response to the second 0 to 50mM NaCl
883 upstep in wild-type animals. The slopes for the second 0 to 50 mM NaCl upstep between
884 wild-type and *gcy-22(tm2364)* animals are different (n = 17 (blue; wild-type), n=23 (teal;
885 *gcy-22*); permutation test p<0.05). In wild-type animals, the slopes in response to the

886 second 0 to 50 mM NaCl upstep are also different from those of the switch control (n= 17
887 (blue; 50 mM NaCl downstep), n=11 (pink; switch control); permutation test p<0.0001).
888
889 **Fig 4. WincG2 expression in ASE does not affect reporter activity but can**
890 **increase NaCl seeking behavior.**
891 (A) Animals were tested for NaCl cultivation preference adapted from Iino [18]. Briefly,
892 animals were placed on cultivation plates with various NaCl concentrations for around six
893 hours before being placed on an assay plate with regions of higher and lower NaCl
894 concentration. (B) Wild-type animals injected with 15 ng/µl *flp-6p*::WincG2 exhibited a
895 preference for higher [NaCl] while maintaining behavioral plasticity; animals from this line
896 were recorded and analyzed for panels C, D, and E. Wild-type animals cultivated at 25mM
897 NaCl, 50mM NaCl, and 100mM NaCl have a chemotaxis index (CI) approaching -1, 0 and
898 0.75, respectively (first three bars). The line injected with 15 ng/µl *flp-6p*::WincG2
899 produces two types of progeny: those that do not express the array (nontransgenic
900 siblings) and those that do (transgenic siblings). Nontransgenic siblings behave like wild-
901 type animals (second three bars) (Welch's t test, ns). Transgenic animals cultivated at
902 each NaCl concentration exhibit a slight but not significant preference for higher NaCl
903 concentration relative to wild-type animals (Welch's t test, ns). (C) Average fluorescence
904 response ($\Delta F/F_0$) of WincG2 in ASER cell body shown as traces responding to ten 10
905 second steps between 50 and 0 mM NaCl (represented at the bottom of the panel).
906 WincG2 fluorescence in wild-type (N2) animals decreases linearly in response to a 50 to
907 0 mM NaCl downstep and stops decreasing in response to a 0 to 50 mM NaCl upstep;
908 this is seen in animals injected with either 7.5 ng/µl (top trace; blue) or 15 ng/µl (bottom

trace; red) *flp-6p*::WincG2. The data for the strain injected with 7.5 ng/µl *flp-6p*::WincG2 are the same data that was used in Fig 4A as wild-type (N2). Regression analysis was applied to the data for the first 50 to 0 mM NaCl downstep. R^2 = 0.9962 and R^2 = 0.9963 for wild type animals injected with 7.5 ng/µl and 15 ng/µl *flp-6p*::WincG2, respectively. (D) The slope values of the first 50 to 0 mM NaCl downstep and 0 to 50 mM NaCl upstep are different in wild-type animals injected with either 7.5 ng/µl (n=17; first pair, blue; permutation test p<0.00001) or 15 ng/µl (n=18; second pair, red; permutation test p<0.00001) *flp-6p*::WincG2. The data for the strain injected with 7.5 ng/µl *flp-6p*::WincG2 are the same as the data used in Fig 4B as wild-type, first pair, blue. The slopes for the first 50 to 0 mM NaCl downstep in wild-type animals injected at 7.5 ng/µl and 15 ng/µl *flp-6p*::WincG2 are not different (n = 17 (blue; 7.5 ng/µl), n=18 (red; 15 ng/µl); permutation test ns).

Fig 5. WincG2 allows visualization of cGMP production in PHB chemosensory neurons in response to the repellent SDS.

(A) Diagram of the PHB circuit [19,32,33]. The primary postsynaptic partners of PHB neurons are the AVA backward command interneurons and the PVC forward command interneurons. (B) Diagram of the sodium dodecyl sulfate (SDS) behavioral assay, which tests the PHB circuit response to 1 mM SDS [19,32,33]. Animals are induced to move backwards with a nose touch from a hair pick. A drop of 1 mM SDS is placed behind them on a dry NGM plate, so that the drop quickly absorbs into the media, preventing wicking along the worm. The time that the animal backs into the drop before stopping is

932 measured. (C) WincG2 does not affect the response of animals to SDS. For reference,
933 loss of *tax-4* cyclic nucleotide-gated channel causes a severe defect in the ability to sense
934 SDS [32]. (D) When WincG2 is expressed in PHB neurons, $\Delta F/F_0$ increases steadily after
935 introduction of 1mM SDS. n=16 (E) The area under the curve for traces before and after
936 SDS presentation is different (permutation test, p<-0.00001).
937
938 **Supporting Information Captions**
939
940 **S1 Fig. Coexpression of bPGC with the cGMP-gated cation channel TAX-2/TAX-4 in**
941 **body wall muscle cells results in muscle contraction within two seconds upon**
942 **exposure to blue light (n=10).** bPGC(K265D) contains a point mutation that abolishes
943 guanylyl cyclase activity. Animals coexpressing bPGC(K265D) with TAX-2/TAX-4 did not
944 contract to the same extent (n=12).
945
946 **S2 Fig. WincG2 fluorescence in the ASER cell body increases in response to the**
947 **third and fourth 0 to 50mM NaCl upstep in wild-type animals.** The difference in slopes
948 for the third and fourth 0 to 50 mM NaCl upstep between wild-type and *gcy-22(tm2364)*
949 animals is significant (n = 17 (blue; wild-type), n=23 (teal; *gcy-22*); permutation test
950 p<0.05 for third upstep and p<0.01 for fourth upstep). In wild-type animals, the difference
951 between the slopes in response to the third and fourth 0 to 50 mM NaCl upstep is also
952 significant from those of the switch control (n= 17 (blue; wild-type), n=11 (pink; switch
953 control); permutation test p<0.01).
954

S3 Fig. Other lines generated from injecting 15 ng/µl *flp-6p*::WincG2 exhibit a preference for higher [NaCl] while maintaining behavioral plasticity. This preference is significantly different from wild-type animals and nontransgenic siblings.

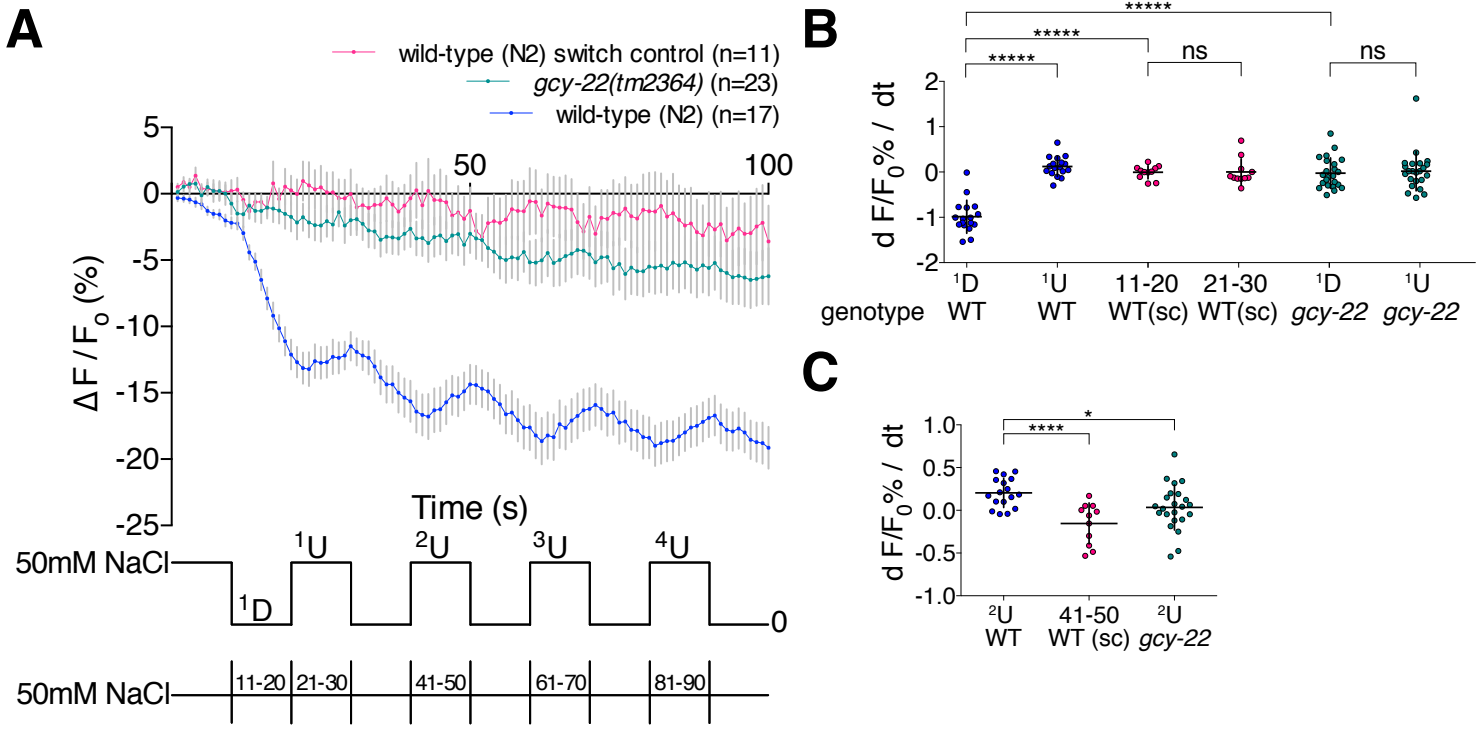
A
wild-type (N2) switch control (n=11)
gcy-22(tm2364) (n=23)
wild-type (N2) (n=17)
ΔF / F0 (%)
Time (s)
50mM NaCl
1D
1U
2U
3U
4U
11-20
21-30
41-50
61-70
81-90
B
d F/F0% / dt
genotype
1D WT
1U WT
11-20 WT(sc)
21-30 WT(sc)
1D gcy-22
1U gcy-22
*****
ns
C
d F/F0% / dt
2U WT
41-50 WT (sc)
2U gcy-22
****
*

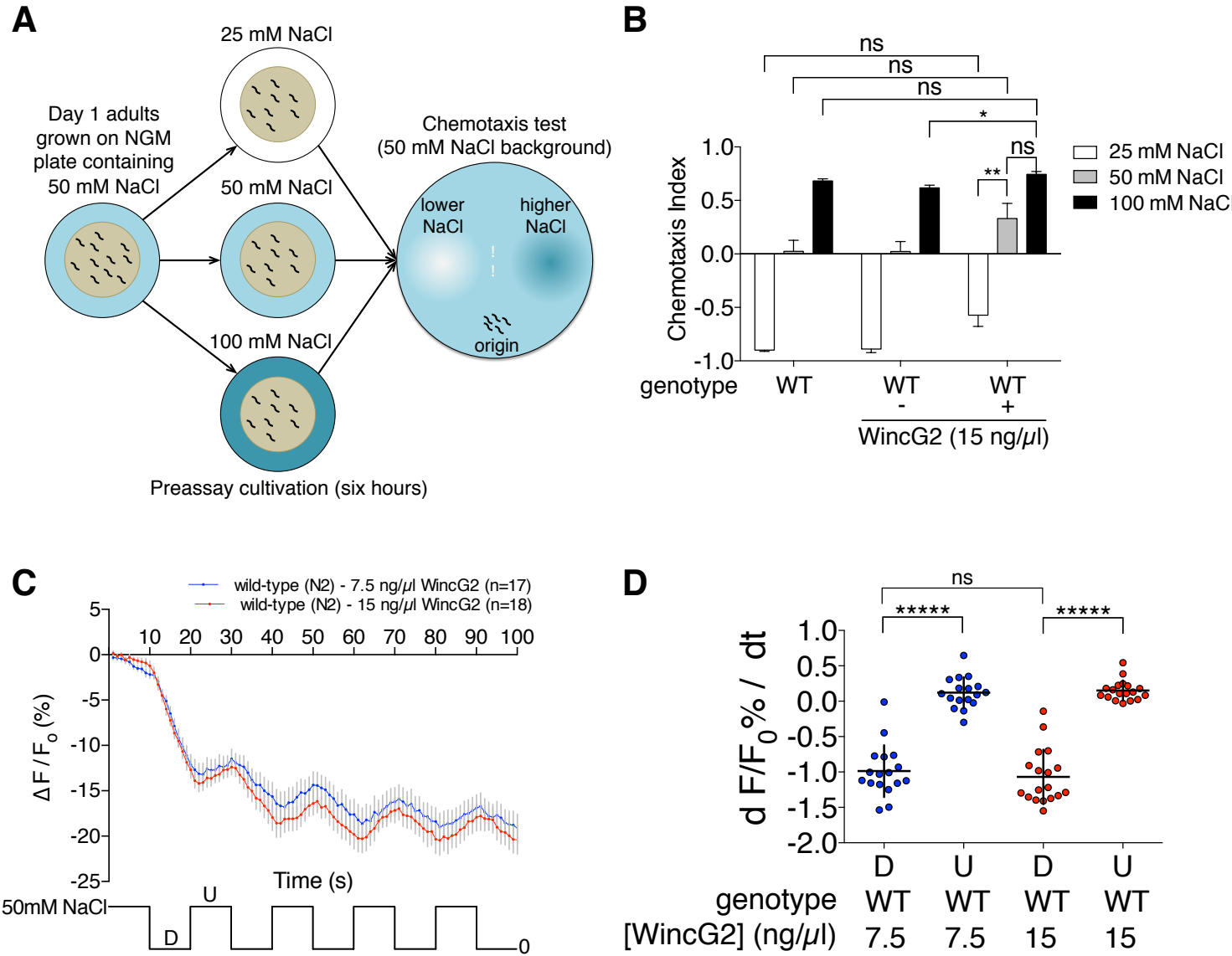
A
25 mM NaCl
Day 1 adults
grown on NGM
plate containing
50 mM NaCl
50 mM NaCl
Chemotaxis test
(50 mM NaCl background)
lower
NaCl
higher
NaCl
origin
100 mM NaCl
Preassay cultivation (six hours)
B
ns
ns
ns
*
ns
**
Chemotaxis Index
1.0
0.5
0.0
-0.5
-1.0
25 mM NaCl
50 mM NaCl
100 mM NaCl
genotype
WT
WT
-
WT
+
WincG2 (15 ng/µl)
C
wild-type (N2) - 7.5 ng/µl WincG2 (n=17)
wild-type (N2) - 15 ng/µl WincG2 (n=18)
ΔF / F0 (%)
5
0
-5
-10
-15
-20
-25
10 20 30 40 50 60 70 80 90 100
Time (s)
50mM NaCl
U
D
0
D
ns
*****
*****
d F/F0% / dt
1.0
0.5
0.0
-0.5
-1.0
-1.5
-2.0
D
U
D
U
genotype
WT
WT
WT
WT
[WincG2] (ng/µl)
7.5
7.5
15
15

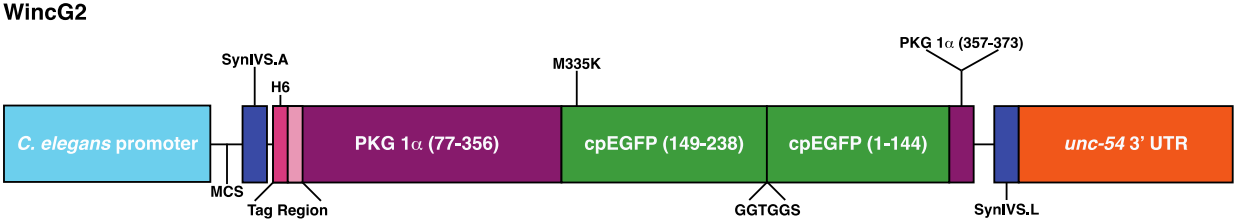
WincG2
SynIVS.A
H6
M335K
PKG 1α (357-373)
C. elegans promoter
PKG 1α (77-356)
cpEGFP (149-238)
cpEGFP (1-144)
unc-54 3' UTR
MCS
Tag Region
GGTGGS
SynIVS.L

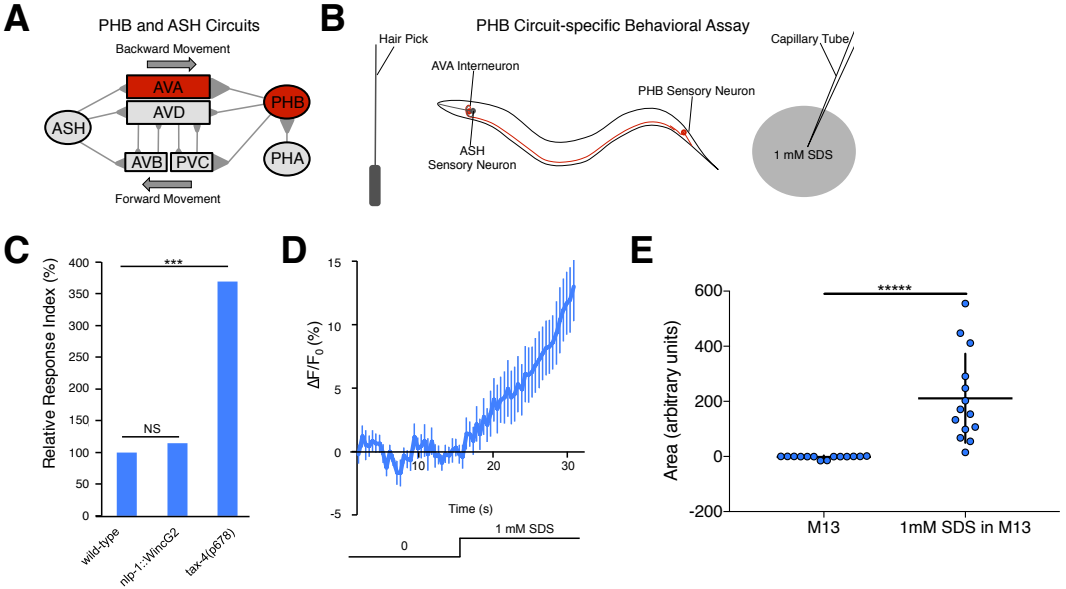
A
PHB and ASH Circuits
Backward Movement
AVA
AVD
PHB
ASH
AVB
PVC
PHA
Forward Movement
B
PHB Circuit-specific Behavioral Assay
Hair Pick
AVA Interneuron
PHB Sensory Neuron
Capillary Tube
ASH
Sensory Neuron
1 mM SDS
C
Relative Response Index (%)
***
NS
wild-type
nlp-1::WincG2
tax-4(p678)
D
ΔF/F0 (%)
Time (s)
1 mM SDS
0
E
Area (arbitrary units)
*****
M13
1mM SDS in M13

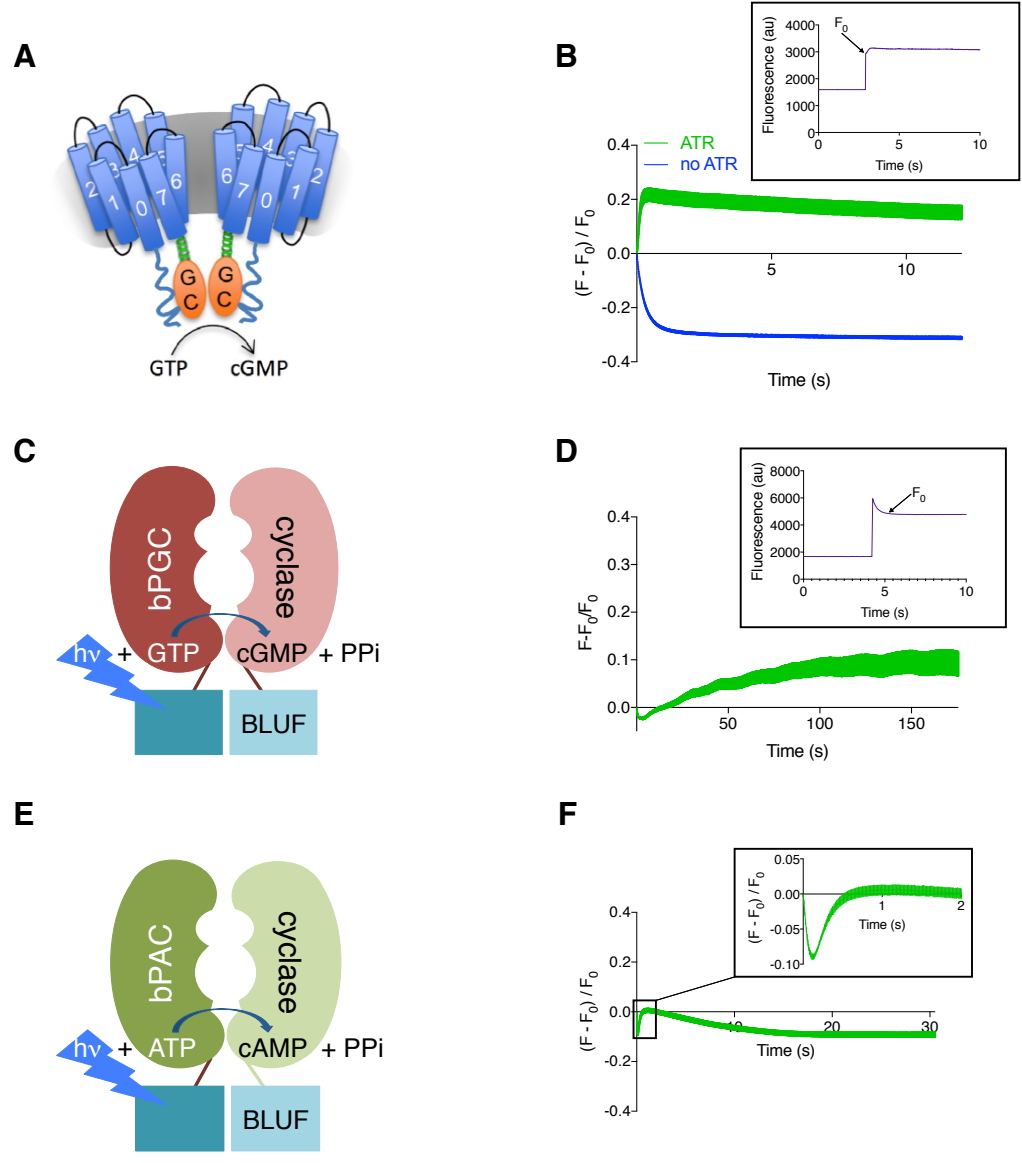
A
B
C
D
E
F
GTP
cGMP
ATR
no ATR
Fluorescence (au)
Time (s)
bPGC
cyclase
hν
GTP
cGMP
+ PPi
BLUF
bPAC
ATP
cAMP